Feng Xu, Xiping Wang*, Marko Teder and Yunfei Liu*

Acoustic impact testing and waveform analysis for damage detection in glued laminated timber

DOI 10.1515/hf-2016-0237
Received December 28, 2016; accepted May 11, 2017; previously published online xx

Abstract: Delamination and decay are common structural defects in old glued laminated timber (glulam) buildings, which, if left undetected, could cause severe structural damage. This paper presents a new damage detection method for glulam inspection based on moment analysis and wavelet transform (WT) of impact acoustic signals. Acoustic signals were collected from a glulam arch section removed from service through impact testing at various locations. The presence and positions of internal defects were preliminarily determined by applying time centroid and frequency centroid of the first moment. Acoustic signals were then decomposed by wavelet packet transform (WPT) and the energy of the sub-bands was calculated as characteristics of the response signals. The sub-bands of 0–375 Hz and 375–750 Hz were identified as the most discriminative features that are associated with decay and delamination and therefore are indicative of the presence of delamination or decay defects. A defect diagnosis algorithm was tested for its ability to identify internal decay and delamination in glulam. The results show that depth of delamination in a glulam member can be determined with reasonable accuracy.

Keywords: decay, delamination, glulam, moment analysis, wave propagation, wavelet transform

Introduction

Glued laminated timber (glulam) is widespread all over the world and extend modern wooden building capabilities. In glulam, timber laminates are stacked and glued together and are able to carry more loads, for instance, in large-span roofs. Glulam constructions are appreciated for their strength, durability and versatility. Modern quality assessment methods are needed to assure or extend the service life of glulam structures, especially in the context of adhesive bonding failures causing delamination in glulam elements.

Delamination usually results from improper bonding, overloading during the service life of a structure or by moisture changes that introduce stresses (Angst and Malo 2010; Bucur 2011; Neuenschwander et al. 2013). Similar to solid-sawn timbers, decay can also occur in glulam members as a result of water intrusion and poor ventilation. Damage from delamination and decay is usually the result of slow processes and a catastrophic failure can be avoided by regular inspections and early detection. However, these types of deteriorations may take place hidden from view and remain undetected. There have been many incidences where glulam structures failed and caused significant property losses and endangered public safety (Hansson and Larsen 2005; Frühwald et al. 2007; Divos 2011; Sitar 2016).

In current practice, structural condition assessment still largely relies on visual surface inspection, which provides only limited information on the internal state concerning the bonding performance of glulam members (Ross et al. 2004; Kasal 2010). Stress wave timing measurement has proved to be effective in predicting the stiffness of structural members and detecting moderate to severe internal rot or cracks in both solid-sawn timber and glulam members; however, it has limited success in identifying early stages of deterioration and local bonding failures (Ross et al. 2004; Senalik et al. 2010; Arriaga et al. 2013; Teder and Wang 2013; Wang et al. 2013). Methods of ultrasonic wave propagation (perpendicular to the grain) have been applied to glulam for assessing the bond quality and resulted in better results in terms of resolution and sensitivity (Maeva et al. 2004; Dill-Langer et al. 2005; Birks et al. 2007; Divos 2011; Sanabria et al. 2011; Xu and Liu 2011). However, the apparatus and operating procedures for ultrasonic inspection in large glulam members are constrained by the low level of the energy source and the coupling issues often encountered in the field (Beall 2002; Dill-Langer et al. 2005; Senalik et al. 2010; Bucur 2011; Sanabria et al. 2011; Neuenschwander et al. 2013). More advanced methods need to be explored

***Corresponding authors: Dr. Xiping Wang,** USDA Forest Products Laboratory, Madison, WI, USA, e-mail: xwang@fs.fed.us; and **Dr. Yunfei Liu,** College of Information Science and Technology, Nanjing Forestry University, Nanjing 2100037, China, e-mail: lyf@njfu.com.cn
Feng Xu: Nanjing Forestry University, Nanjing, China
Marko Teder: Estonian University of Life Sciences, Tartu, Estonia

and developed for the field inspection of glulam components in modern buildings.

Several non-destructive testing techniques (stress wave timing, ultrasonic transmission, resistance micro-drilling) were already tested to assess the physical conditions of glulam arches removed from a service building (Teder and Wang 2013). The objective of the present study was to explore the possibilities and limitations of an acoustic impact testing method coupled with two advanced waveform analysis techniques, i.e. moment analysis and wavelet transform, to detect delamination and internal decay in glulam arches.

Backgrounds

Moment analysis is one of the most applied signal processing methods by which many signal features can be obtained. In general, when a signal is excited and transmitted in a flawless medium, most of its energy is typically located in the beginning of the signal waveform. Reflection and mode changes of a signal often come from the boundaries and material flaws, causing the skewing of the signal in the time domain. Therefore, moment analysis should be able to characterize the damage of a material. Tiitta et al. (1998) applied time centroid (TC) and frequency centroid (FC) (a form of the first moment) of the acousto-ultrasonic signals in laboratory experiments as inputs of the neural network classifier for decay detection in brown-rotted Douglas fir glulam. A 79% efficiency was found for detecting small levels of decay and a 68% efficiency for the overall accurate classification of different degrees of decay. Bayissa et al. (2008) applied a damage detection technique based on the statistical moments of the energy density function of the vibration responses in the time-scale domain. The zeroth-order moment, known as the total energy of the joint density function, was computed at each measurement grid point for the pre-damage and post-damage states and applied to locating structural damage in a concrete plate model and separately in a steel plate girder of a bridge. The robustness of the proposed damage identification for real-world applications has been verified by means of experimental modal data from a full-scale bridge structure subjected to various damage condition states and random vibration excitations.

The wavelet transform (WT) of a signal is another useful tool for time-frequency domain analysis, which characterizes time-frequency variations of the signal sub-band components. The WT approach is suitable for analyzing non-stationary signals with transient and time-varying characteristics, in the course of which both time and frequency domains can be characterized simultaneously. In the meanwhile, this technique has been widely implemented for various unique purposes, such as de-noising of signals, information retrieval from noise-polluted signals, classification and pattern recognition applications (Mallat 1999; Brenner 2003; Bayissa et al. 2008), characterization of non-stationary dynamic responses (Basu and Gupta 1997; Xu and Liu 2011, 2014) and identification of nonlinear structural dynamic systems (Kitada 1998).

The WT application for damage identification and health monitoring has also been reported. Liu et al. (2010) presented a crack detection method for fiber-reinforced composite beams based on continuous WT (CWT); the authors found that the crack location could be determined successfully and the crack depth could be estimated from the crack-reflection ratio. Rucka (2011) applied a WT-based damage detection technique on a cantilever beam, where the damage was present in the form of a single notch at depths of 20, 10 and 5% of the beam height. The conclusion was that the smallest detectable defect was at a 10% depth of the beam height, and defect location can only be determined by higher vibration modes. Umesha et al. (2009) proposed an analytical method for locating and quantifying the damage in fixed beams with a single crack by WT analysis, and demonstrated that the method could locate and quantify the damage in beams or beam-like structures without prior knowledge of the deflection corresponding to the undamaged structure. Although the quoted papers reported satisfactory results, they were mostly focused on numerical analysis of ideal models and experimental analysis of isotropic materials with ideal and single flaws. Very little information is available for the application of WT analysis in glulam structure inspection. The challenge is that the response signals in glulam members are more complicated than those in ideal experimental materials.

Materials and methods

The glulam arch member investigated here was salvaged from a research building at the USDA Forest Products Laboratory (FPL) that was deconstructed in the fall of 2010, after more than 75 years of service. Originally built as a test and storage facility, the building is considered to be the second oldest glulam structure in the United States (US) (Rammer et al. 2014). In Figure 1, I is an inside view of the building showing the solid glulam arches at the middle bays. The building was 14 m wide, 3.7 m high at the walls and 5.8 m high at the center. The halves of the glulam arches were bent at the knee but were straight below and above the knee and were held together at the apex with bolted plates. The arches in this structure represent

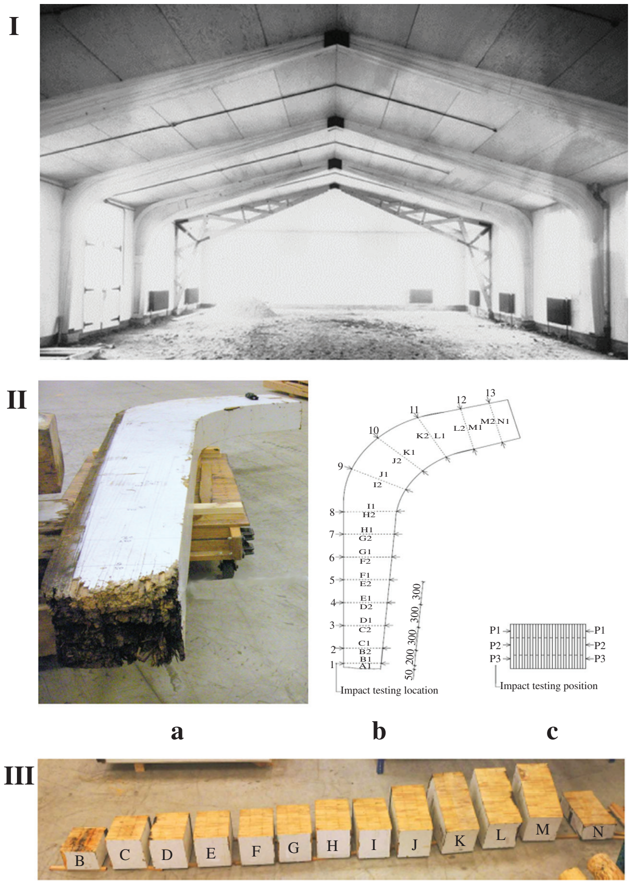

Figure 1: Glulam arch member removed from service was investigated by acoustic impact testing.
I – Building 2, Forest Products Laboratory, Madison, Wisconsin, c. 1935, considered to be the second oldest glulam structure in the US. The solid glulam arches are shown in the middle bay. II – Acoustic impact testing on a glulam arch member. (a) Photo of the glulam arch section cut from arch 5; (b) plan view showing impact testing locations along the glulam length (measured along the inner face of the arch); (c) cross-sectional view showing three testing positions (P1, P2 and P3) along the width. III – The glulam blocks after cross-cutting at each testing location. Block A (not shown) was severely decayed and delaminated and fell into pieces following cutting.

the first generation of both construction adhesives and glulam development in the US and, therefore, the removed glulam arches were preserved as research specimens for various groups at FPL to evaluate the durability and residual strength of these aged arch members (Teder and Wang 2013; Rammer et al. 2014). The solid glulam arches of rectangular cross section were glued and stacked with laminations of 1.4-cm material to a constant width of 29.2 cm, tapering from a maximum depth of 61 cm at the knee, near the junction of wall and roof, to lesser depths at the foundation (30.5 cm) and the roof peak (20.3 cm). Each layer was made of 10.2-cm and 20.3-cm wide southern yellow pine lumber, with the edge joints staggered in alternate laminations (Teesdale 1935).

The general physical conditions of all the solid glulam arch members removed from the building were determined through a preliminary stress wave and ultrasonic timing inspection (Teder and Wang 2013). Glulam arch 5 (Figure 1, IIa) contained a wide range of decay and delamination due to moisture intrusion and exposure to elevated temperatures in the 1993 fire incident. A 3.75-m long section (measured from the base and along the inner face of the arch) was cut from this arch member as a specimen for an extensive acoustic impact testing.

Acoustic impact testing: Figure 1, IIb and IIc show the locations (along the length) and positions (across the width) where acoustic signals were collected. The physical condition of the arch section varied lengthwise; thus, the impact testing was started at the cross section 5 cm from the decayed end (base), followed by a 20-cm increment and then by a 30-cm increment. At each of these locations, acoustic signals were collected at three positions, which were designated as P1, P2 and P3 (Figure 1, IIc). Positions P1 and P3 were each 5 cm away from the edge and position P2 was located in the middle of the width. The impact tests were conducted through the depth of the glulam (perpendicular to the laminations), while the arch section was placed in flat (Figure 1, IIa). Sensor probes (Fakopp Microsecond Meter sensors, Fakopp Enterprise, Ágfalva, Hunary) were inserted into opposing faces of the glulam at the same cross section and same position level. Acoustic waves were generated through a hammer impact. The response signals were collected via a data acquisition card NI 5132 connected to a laptop, with a sampling frequency of 12 kHz.

Upon completion of acoustic impact testing, the glulam specimen was dissected at each testing location, resulting in 14 glulam blocks labeled A–N (Figure 1, III). Block A was severely decayed and delaminated and fell into pieces following cutting. Visual inspection was conducted at each opened cross section to identify decay, delamination and any cracks that could be obviously seen. Decay was identified by detecting color changes, loss of wood and lack of probing resistance in the pick test. Delamination and cracks were identified by observing visible separation. A high-resolution digital image of each cross section was subsequently obtained to document the internal conditions of the glulam section.

Signal processing and analysis: First, the time-energy centroid (TEC) and frequency-energy centroid (FEC) of the acoustic signals were obtained through moment analysis. The TEC indicates the time at which most of the signal energy has been received. Mathematically, TEC (t_E) is the first moment of the square of a signal with respect to time divided by the zeroth moment with respect to time:

$$t_E = \frac{\sum_{i=1}^{N} A_i^2 t_i}{\sum_{i=1}^{N} A_i^2} \tag{1}$$

where N is the number of time samples, A_i is the amplitude of the i^{th} time step and t_i is the time at the i^{th} time step. The FEC is defined as:

$$f_E = \frac{\sum_{i=1}^{N_f} S_i^2 f_i}{\sum_{i=1}^{N_f} S_i^2} \tag{2}$$

where f_E denotes FEC, N_f is the number of frequencies in the spectrum and S_i and f_i are the amplitude and frequency of the i^{th} frequency of the spectrum, respectively. The centroid parameters were examined as potential defect predictors through preliminary analysis. The predicted defects were then compared with the actual conditions of the cut-opened cross sections.

Second, the acoustic signals were decomposed by means of wavelet packet transform (WPT) and the energy of the sub-bands was deduced as characteristics of the response signals. In mathematics, WT is a breaking up of a signal into shifted and scaled versions of a mother wavelet or base function. This results in variable sizes of a window function and makes it possible to detect discontinuities and breakdown points of data that other analysis methods usually miss (Kim and Melhem 2004). WPT can be viewed as a natural extension of the WT, decomposing a signal repeatedly into successive low-frequency (LF) and high-frequency (HF) components. The only difference between WPT and WT is that WPT decomposes not only the approximation but also the details at a given level; therefore, it is more flexible and has a wider base for the analysis of signals (Mallat 1999; Taha et al. 2006). WPT also enables multi-resolution damage detection as it can localize multi-frequency bands in the time domain. In this paper, the response signals collected from the glulam arch section were decomposed into four levels by WPT with a mother wavelet "db 3" (one of the wavelet functions of Daubechies family), and the wavelet packet coefficients at the fourth level were reconstructed, respectively. The energy ratio (ER, defined as percentage of the energy of each scale component decomposed) was calculated as the feature vector to identify different types of sound sources. The characteristic differences of the response signals can be compared by computing the ER of each leaf at the fourth level and drawing a time-frequency distribution map and a wavelet packet spectrum of the decomposed signal.

Following the WPT of the response signals, the feature differences concerning the signals associated with typical defects and those associated with intact cross-sections were analyzed, and the sub-bands that can serve as diagnostic criterion for the presence of defects were identified. Based on the identified features, the possibilities for the presence of defects at all testing locations were analyzed and determined.

Finally, based on the time-frequency distribution obtained through the WPT, the transmission time differences were further analyzed for the sub-band components of the signals from the damaged and solid sections, and approximate velocity relations were determined in terms of the sub-band components between the signals. A defect diagnosis algorithm will then be proposed to predict the nature and sizes of the defects based on the transmission characteristics and the geometric path of the wave propagation.

Results and discussion

Time-energy and frequency-energy centroids

Figure 2 shows the time-domain signals (a), frequency spectra of the signals (b), time-frequency distributions (c), frequency sub-band distribution (d) and the cross-sectional images (e) for three representative locations (1, 2, and 13; all at P1 position) in the glulam arch section. The cut-opened cross sections revealed severe damage (including decay and delamination) at location 1 (Figure 2, Ie), moderate decay and delamination at location 2 (Figure 2, IIe) and intact condition at location 13 (Figure 2, IIIe). Both time-domain signals and the frequency spectra show distinct differences among these locations. It appears that decay and delamination caused a noticeable decrease in the time-domain signal. In the frequency domain, the main frequency contents shifted to the LF region, when the glulam arch progressively deteriorated. Comparing with the solid cross section (location 13), the HF content of the signal was absent at locations 1 and 2, and the amplitude of the peak frequencies was also substantially reduced (Figure 3). These observations are consistent with the results reported by Tiitta et al. (1998) and Senalik et al. (2008).

Figure 4 shows the distribution of TEC and FEC of the response signals collected at 13 locations of the glulam arch section. The TEC value at the three positions (P1, P2 and P3) showed very little variation throughout the entire glulam arch section. However, a significant change in the TEC value was observed along the length. TEC remained relatively constant (0.0076–0.01 s) from locations 3 to 13, but increased to 0.025 and 0.030 s at locations 2 and 1, representing a 150% and 200% increase, respectively. Clearly, the damages at locations 1 and 2 caused significant delay in the arrival of the bulk signal energy.

On the other hand, the FEC values show opposite trends along the length, with low frequencies (1 kHz and less) observed at locations 1 and 2 and high frequencies (above 1250 Hz) at the remaining locations. The absence of high frequencies at locations 1 and 2 is the indication that high-frequency components had been attenuated sharply, when acoustic waves transmitted through the glulam cross section, which implies that the laminates at those locations had a much lower density compared to the intact laminates at other locations, as a result of the deterioration confirmed by the cut-opened cross sections (Figure 2, Ie and IIe). It is also noted that, from location 2 onwards, the FEC value at position P1 was consistently lower than the values at positions P2 and P3, a hint of a possible early stage of material deterioration at P1 side relative to positions P2 and P3. This could have been caused by the high temperature exposure at that side of the arch during the fire incident in 1993 (Teder and Wang 2013), evidenced by the cross-sectional images and visual observation of the small delamination.

Another interesting finding is that the FEC of the response signals at location 9 position P3 and location 10 positions P1, P2 and P3 fell sharply, but the corresponding TEC basically remained unchanged. A visual assessment of the corresponding cross sections following cross-cutting revealed some small delamination at location 9 (Figure 5a) and longer delamination at location 10 (Figure 5b). This indicates that the FEC of the response signals is more sensitive to the presence of small delamination than the TEC.

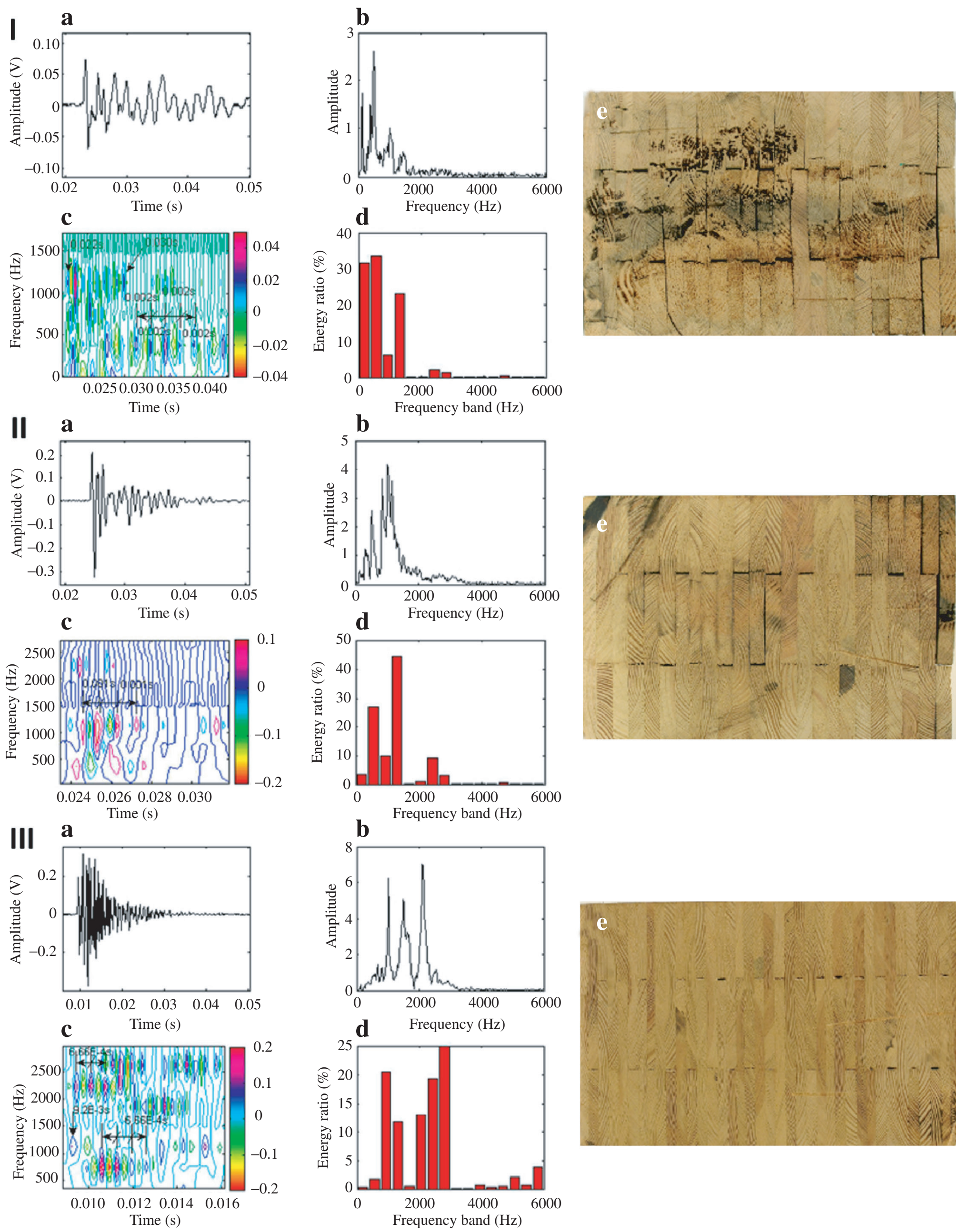

Figure 2: Features of the acoustic signals received from locations 1, 2 and 13 and the corresponding cross-sectional images of the glulam arch section. I – Location 1 (with severe decay and delamination); II – Location 2 (with moderate decay and delamination); III – Location 13 (intact). (a) Time-domain response signal from testing point P1; (b) frequency spectrum of the response signal; (c) time-frequency distribution; (d) frequency sub-band distribution; and (e) cross-sectional images of the glulam arch section.

A comparitive analysis of all 13 locations clearly indicated that variations of both the TEC and FEC values reflected physical conditions of the glulam arch section and therefore are good predictors for detecting the presence of internal defects. However, from the time-domain and frequency-domain analyses of the non-stationary acoustic signals, it is difficult to ascertain the nature of defects. Therefore, it is necessary to apply the WT method to further decode response signals and extract new features through time-frequency analysis.

Energy distribution of wavelet sub-bands

Figure 6 shows the ERs of wavelet sub-bands of the response signals at the 13 testing locations. The following

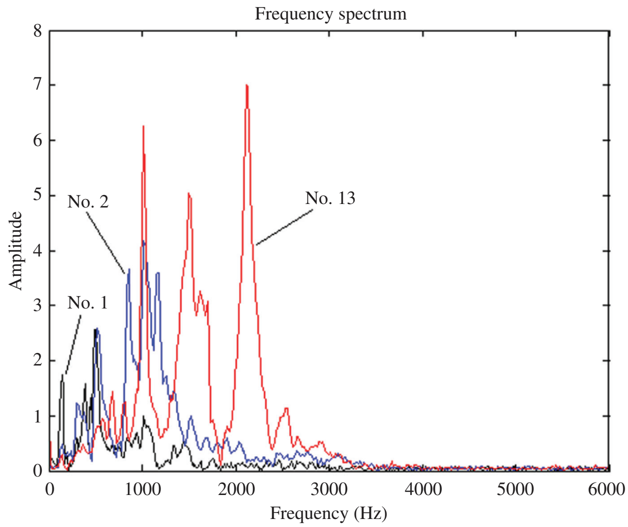

Figure 3: Three frequency spectra overlaid showing the frequency shift from the higher to lower frequencies with increasing damage (location 1 – with severe decay and delamination; location 2 – with moderate decay and delamination; and location 13 – intact).

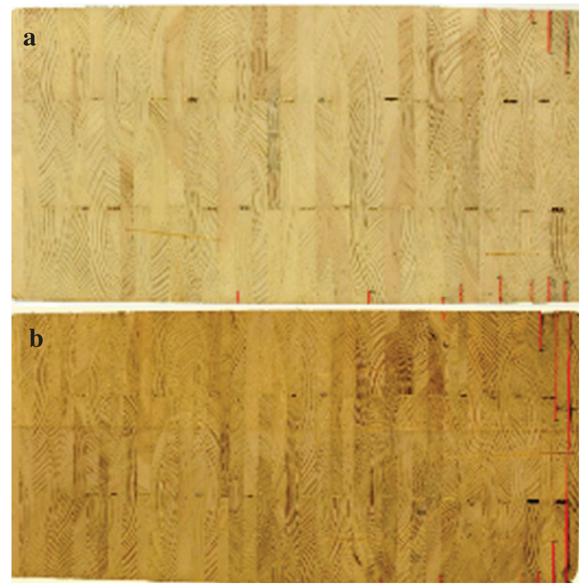

Figure 5: Cut-open cross-sectional images of the glulam arch section at location 9 (a) and location 10 (b).
Red lines indicate visually observed delamination.

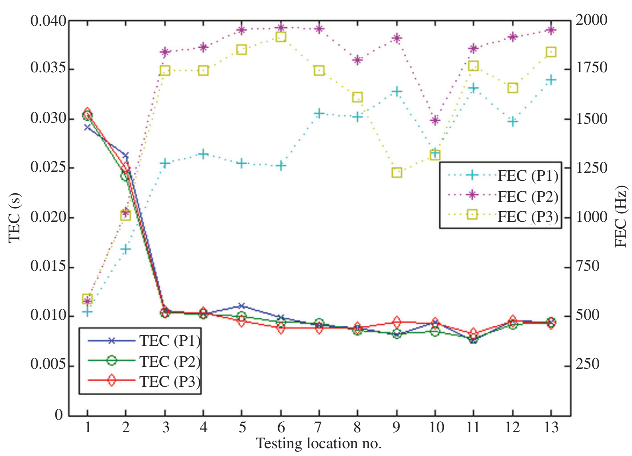

Figure 4: Time-energy centroid (TEC) and frequency-energy centroid (FEC) of the response signals at various testing locations.

discussion will be focused on three representative signals from locations 1, 2 and 13 to illustrate the proposed method. The response signal received at location 1 (Figure 2, Ia) corresponds to the cross section that contained severe defects (decay and delamination as illustrated in Figure 2, Ie). The distribution of frequency sub-bands (Figure 2, Id) indicates that the signal energy is primarily concentrated in the LF range. The combined energy for the two LF sub-bands (LF1: 0–375 Hz and LF2: 375–750 Hz) accounts for 64% of the total energy of the response signal. The ER of the LF1 sub-band reached 31.8%. In contrast, the ERs of the middle-frequency (MF) sub-bands (MF1: 750–1125 Hz and MF2: 1125–1500 Hz) are 6.18% and 23.5%, respectively, and the ER of the HF component (>1.5 kHz) accounts for <5%.

The response signal received at location 2 (Figure 2, IIa) corresponds to the cross section that contained moderate deterioration (early-to-moderate decay and partial delamination, see Figure 2, IIe). The distribution of the frequency sub-bands (Figure 2, IId) shows that the signal energy is mostly concentrated in the MF range. The ERs of the sub-bands LF1 (0–375 Hz) and HF (>1.5 kHz) are 3.4% and 14.8%, respectively. The ERs of the sub-bands of 375–750 Hz, 750–1125 Hz and 1125–1500 Hz are 27.1%, 10.1% and 44.6%, respectively. Compared to the response signal associated with severe defects (Figure 2, I), the distribution of the frequency sub-bands presented in Figure 2, IId has the following features: the energy of the LF1 component (0–375 Hz) dropped significantly, while the MF components increased considerably. In addition, the HF sub-band increased as well.

For the response signal without defects (Figure 2, IIIa for location 13), the frequency sub-bands have a very unique distribution. The ERs of the LF sub-bands of 0–375 Hz and 375–750 Hz are very low, only 0.3% and 1.7%, respectively. Meanwhile, the ERs of the MF sub-bands of 750–1125 Hz and 1125–1500 Hz are relatively high, 20.5% and 11.8%, respectively. The most important observation is that the ER of the HF sub-band (>1.5 kHz) is the highest, reaching 65.7%.

The ERs of wavelet sub-bands of the response signals obtained from different locations (along length direction)

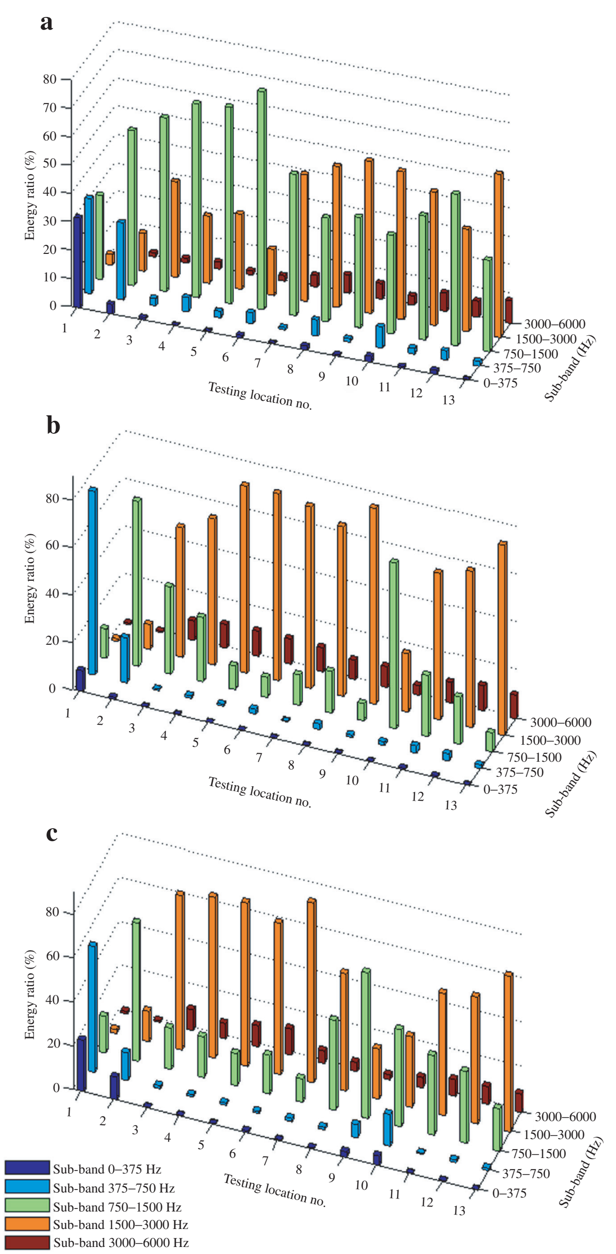

Figure 6: Energy ratios of wavelet sub-bands of the response signals at 13 testing locations.
(a) Position P1; (b) position P2; and (c) position P3.

and different positions (P1, P2 and P3) are summarized in the bar graphs in Figure 6. The high ERs of the LF bands at locations 1 and 2 are clearly associated with the severe-to-moderate deterioration as revealed by the cross-sectional images (Figure 2, Ie and IIe). Locations 9 and 10 have slightly higher than normal ERs of the LF components in P3 (5% increase in comparison with sound sections), indicating a possible deterioration in these areas. A visual examination of the cross sections revealed some partial delamination at different depths at these locations (Figure 5).

Analysis of frequency sub-bands indicates that the internal condition of a glulam member could have a significant impact on the signal energy distribution. When severe decay occurred, the energy of the response signal was heavily concentrated on the first LF sub-band (LF1: 0–375 Hz), while that of the second LF sub-band (LF2: 375–750 Hz) could be related to early decay or delamination. HF sub-bands of >1.5 kHz are indicative of sound timber; i.e. the higher the ER of the HF components, the better is the quality of the glulam member. Consequently, it can be safely concluded that the sub-band energy distribution of a response signal from wavelet analysis is an indicator of internal soundness.

Time-frequency spectrum analysis

Figure 2, Ic, IIc and IIIc are the time-frequency spectra of the response signals collected at three representative locations 1, 2 and 13. The color indicates the amplitudes of the frequency components (color scale is presented in the secondary Y-axis). These figures illustrate both intensity of the frequency components and their distribution. For location 1, which contained advanced decay and delamination, energy distribution of the MF2 (1125–1500 Hz) and LF sub-bands are explicitly presented in Figure 2, Ic. The receiving time of the response signal is at 0.02233 s. After 0.03 s, the LF sub-bands are still stable in transmission and their amplitudes are basically unchanged. The LF2 (375–750 Hz) component appeared regularly at an interval of 0.002 s (Δt_1). In contrast, the HF sub-bands are nearly not visible and the MF components show an obvious attenuation.

For location 2, which had moderate decay and partial delamination, the response signal was received at 0.024 s. The LF sub-band (0–375 Hz) is almost nonexistent. The HF component was observed in the beginning, but then dropped dramatically after 0.03 s and was hardly visible. Meanwhile, both the LF2 (375–750 Hz) and MF2 (1125–1500 Hz) components were present steadily and their amplitudes are unchanged. The MF2 component appears regularly at an interval of about 0.001 s (Δt_2).

For the intact cross section at location 13, the response signal was received at 0.0092 s, much earlier than those at locations 1 and 2. The frequencies of the signal are mainly in the MF1 (750–1125 Hz) and HF (>1.5 kHz) sub-band regions, while LF1 (0–375 Hz) was almost missing. All frequency sub-bands are stable with less attenuation

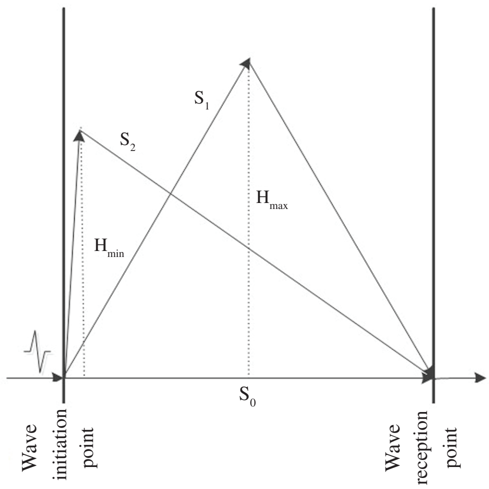

Figure 7: Wave propagation path across the depth of a glulam member with an artificial delamination.
S_0, S_1 and S_2 represent three possible propagation paths. S_0: reference path with no defect; S_1: detour for a delamination located in the middle of the beam (with the maximum depth $H_{max}=1.414\ S_0$); and S_2: detour for a delamination located near the boundary (with the minimum depth $H_{min}=1.333\ S_0$).

in transmission, and appear almost at an equal interval of 0.000666 s (Δt_3), which indicates that the acoustic waves propagate at a velocity that is governed by the material itself, independent of the signal frequency.

Assuming that the glulam member is homogeneous (a hypothetical assumption), the velocity ratio among locations 1, 2 and 13 can be estimated based on the time intervals of the appearances of the sub-band components, which is approximately 1:2:3 ($1/\Delta t_1$:$1/\Delta t_2$:$1/\Delta t_3$). This estimation is consistent with the velocity ratios determined by the stress wave timing method reported by Teder and Wang (2013).

Nature and sizes of defects

It is obvious from the time-frequency spectrum analysis that the response signal from location 1 is dominated by LF components, while the HF components nearly vanished. This means that large defects must have been present in the wave propagation paths. These defects absorbed so much of the HF energy components that the HF waves simply disappeared.

For intact glulam, the wave propagation path can be assumed to be a straight line across the glulam depth, represented by the shortest distance (S_0) between the initiating point and the receiving point (Figure 7). In comparison, the perceived wave propagation distance (S_1 or S_2) at the cross section of location 1 with severe deficiencies (assuming only delamination without decay) should triple the reference distance (S_0, 36.8 cm at location 3) according to the estimated velocity ratio. With a tripled wave propagation distance, a single delamination may range from a minimum depth of 49.1 cm, if it is close to the boundary ($H_{min}=1.333\ S_0$), to a maximum depth of 52.0 cm, if it is located in the middle ($H_{max}=1.414\ S_0$) (Figure 7). In fact, the glulam arch was only 29.4 cm wide, i.e. much less than the predicted delamination depth; therefore, the hypothesis of a single delamination should be rejected. This led to a conclusion that in addition to delamination, an advanced decay occurred, which is consistent with the conclusion drawn previously.

At location 2, a similar analysis was applied and it was found that in case of delamination it may range from 14.1 cm to 19.7 cm in depth, which is a realistic scenario. But the high velocity ratio could also indicate a scenario of internal decay. In this case, it is necessary to examine the time-frequency distribution (Figure 2, IIc). As discussed above, the response signal from severely decayed glulam exhibits a clear sub-band of 0–375 Hz. If the response signal shows this LF component, the glulam member must have suffered a significant internal decay, and the length of the supposed delamination cannot be determined. Conversely, in the absence of an internal decay, the delamination size could be estimated. For location 2, the time-frequency spectrum contained the 0–375 Hz component. It is concluded that both delamination and decay are present in this location and, thus, the delamination size cannot be determined.

For location 3, the size of the delamination was estimated to be in the range of 2.7–7.7 cm. But the time-frequency distribution of the response signal contained almost no LF1 component, i.e. the energy of the 0–375 Hz component only accounted for 0.8% of the total signal energy (Figure 6). It is therefore hypothesized that the depth of delamination should be between 2.7 cm and 7.7 cm. Examination of the cross section of location 3 confirmed that the delamination was about 4.5 cm deep.

The depth of delamination at other locations was estimated by the same method and the results are listed in Table 1. Most of the estimations are generally consistent with the measured values except the ones at location 6 position P2 and location 8 position P2, where delamination was not observed visually. The percentage errors are <20% and the minimum error was only about 3%. The multiple delamination parallel to each other was considered as a single one. The calculated value of delamination depth should be considered as the maximum or accumulative value of the major delamination actually existing at each cross section.

Table 1: Predicted and measured depths of delamination in the glulam arch section.

Location	Position	H_{max} (cm)	H_{min} (cm)	H_m (cm)	Prediction error (%)	Visual assessment of cross section
No. 1	P1					
	P2					Severe decay + delam
	P3					
No. 2	P1					
	P2					Moderate decay + delam
	P3					
No. 3	P1	7.70	2.68	4.50	15.3	Delamination
	P2					Intact
	P3					Intact
No. 4	P1	12.64	6.32	9.75	2.8	Delamination
	P2					Intact
	P3					Intact
No. 5	P1	10.51	4.37	9.05	17.8	Delamination
	P2					Intact
	P3					Intact
No. 6	P1	12.17	5.44	8.55	3.0	Delamination
	P2	6.87	1.86	[a]		No visual sign of delam
	P3					Intact
No. 7	P1					Intact
	P2					Intact
	P3					Intact
No. 8	P1	12.96	5.70	9.10	2.50	Delamination
	P2	8.35	2.51	[a]		No visual sign of delam
	P3					Intact
No. 9	P1					Intact
	P2					Intact
	P3	[b]	[b]			Delamination
No. 10	P1	[b]	[b]			Delamination
	P2	[b]	[b]			Delamination
	P3	[b]	[b]			Delamination
No. 11	P1	8.47	2.33	6.50	16.9	Delamination
	P2	8.92	2.57	6.50	11.6	Delamination
	P3					Intact
No. 12	P1	14.27	6.77	9.50	10.7	Delamination
	P2	9.19	3.01	7.50	18.7	Delamination
	P3					Intact
No. 13	P1					Intact
	P2					Intact
	P3					Intact

H_{max}, maximum depth of delamination; H_{min}, minimum depth of delamination; H_m, measured depth of delamination; prediction error $E = \frac{(H_{max} + H_{min})/2 - H_m}{H_m} \times 100\%$.

[a]No delamination observed visually.

[b]Depth of delamination could not be determined for decay existence in glulam arch section or invisible cracks.

Conclusions

TEC and FEC of the first moment are good indicators of the presence of internal defects in glulam members. Higher TEC and smaller FEC indicate a greater probability of the presence of defects. FEC is more sensitive to small defects than TEC. There is a link between sub-band energy distribution of response signals and internal defects of a glulam member. With increasing decay/delamination, the dominating energy of the response signal was gradually shifted from the HF bands to MF and LF bands. The sub-band energy distribution is a good indicator of internal damages such as delamination or decay in glulam members. The energy distributions of wavelet sub-bands are more sensitive to defects than the first moment parameters. The LF sub-bands of 0–375 Hz and 375–750 Hz are the most effective discriminative features associated with internal damage and the HF bands are indicative of sound timber. In addition, the ERs of the sub-bands are related to the extent of damage. The higher the ER of the HF components, the better is the quality of the glulam member. The local time-frequency characteristics of the wavelet packet can be used to determine the velocity ratios relative to the velocity in intact glulam. The nature of defects can also be preliminarily ascertained by analyzing the velocity ratio and energy distributions of the wavelet sub-bands. In cases where only delamination exist in the glulam beam, the depth of delamination could be estimated based on the velocity ratio.

Acknowledgments: This research was conducted through cooperation between the USDA Forest Service Forest Products Laboratory (FPL), Nanjing Forestry University (NFU) and the Estonian University of Life Sciences, and was supported in part by the Priority Academic Program Development (PAPD) of Jiangsu Higher Education Institutions, the NFU Innovation Grant for Outstanding PhD Dissertations (grant 163070682) and the Foundation Archimedes European Social Fund DoRa programme. The authors acknowledge the technical support of the Engineering Mechanics and Remote Sensing Laboratory (EMRSL) at FPL.

References

Angst, V., Malo, K.A. (2010) Moisture induced stresses perpendicular to the grain in glulam: review and evaluation of the relative importance of models and parameters. Holzforschung 64:609–617.

Arriaga, F., Esteban, M., Iñiguez-Gonzalez, G., Bobadilla, I., Liana, D.F., Gonzalez-Sanz, M. (2013) Structural assessment of the timber structure of the Casa Grande building in the Real Cortijo de San Isidro, Aranjuez, Madrid (Spain). In: Proceedings of the 18th International Nondestructive Testing and Evaluation of Wood Symposium, Madison, Wisconsin, USA. pp. 233–244.

Basu, B.B., Gupta, V.K. (1997) Non-stationary seismic response of MDOF systems by wavelet transform. Earthquake Eng. Struc. 26:1243–1258.

Bayissa, W.L., Haritos, N., Thelandersson, S. (2008) Vibration-based structural damage identification using wavelet transform. Mech. Syst. Signal Pr. 22:1194–1215.

Beall, F.C. (2002). Overview of the use of ultrasonic technologies in research on wood properties. Wood Sci. Technol. 36:197–212.

Birks, A.S., Green, R.E., Mclntire, P. Nondestructive Testing Handbook (3rd edition), Vol. 7. Ultrasonic Testing. American Society for Non-destructive Testing, Columbus, OH, 2007.

Brenner, M.J. (2003) Non-stationary dynamics data analysis with wavelet-SVD filtering. Mech. Syst. Signal Pr. 17:765–786.

Bucur, V. Delamination in Wood, Wood Products and Wood-Based Composites. Springer, Berlin, Germany, 2011.

Dill-Langer, G., Bernauer, W., Aicher, S. (2005) Inspection of gluelines of glued-laminated timber by means of ultrasonic testing. In: 14th International Symposium on Nondestructive Testing of Wood, Eberswalde, Germany. pp. 49–60.

Divos, F. (2011) Delamination evaluation of in-service glulam beams and other structural members via ultrasonics. In: Delamination in Wood, Wood Products and Wood-based Composites. Ed. Bucur, Springer, Berlin, Germany. pp. 353–364.

Frühwald, E., Toratti, T., Thelandersson, S., Serrano, E., Emilsson, A. Design of Safe Timber Structures – How Can We Learn from Structural Failures in Concrete, Steel and Timber? Report TVBK-3053, ISSN 0349-4969. Lund University, Lund, Sweden, 2007.

Hansson, H., Larsen, H.J. (2005) Recent failures in glulam structures and their causes. Eng. Fail. Anal. 12:808–818.

Kasal, B. (2010) In-situ assessment of structural timber: state-of-the-art, challenges and future directions. Adv. Mat. Res. 133–134:43–52.

Kim, H., Melhem, H. (2004) Damage detection of structures by wavelet analysis. Eng. Struct. 26:347–362.

Kitada, Y. (1998) Identification of nonlinear structural dynamic systems using wavelets. J. Eng. Mech.-ASCE 124:1059–1066.

Liu, Y., Li, Z., Zhang, W. (2010) Crack detection of fibre reinforced composite beams based on continuous wavelet transform. Nondestr. Testing Eval. 25:25–44.

Maeva, E., Severina, I., Bondarenko, S., Gr Maev, R. (2004) Acoustical methods for the investigation of adhesively bonded structures: a review. Can. J. Phys. 82:981–1025.

Mallat, S. A Wavelet Tour of Signal Processing, 2nd ed. Academic Press, London, UK, 1999.

Neuenschwander, J., Sanabria, S.J., Schuetz, P., Widmann, R., Vogel, M. (2013) Delamination detection in a 90-year-old glulam block with scanning dry point-contact ultrasound. Holzforschung, 67:949–957.

Rammer, D.R., Moura, J.M., Ross, R.J. (2014) Structural performance of the second oldest glued laminated structures in the United States. In: Proceeding of the Structures Congress 2014. April 3–5, 2014, Boston, Massachusetts, USA. Structural Engineering Institute of ASCE, Reston, VA, USA. pp. 1233–1243.

Ross, R., Brashaw, B.K., Wang, X., White, R.H., Pellerin, R.F. Wood and Timber Condition Assessment Manual. Forest Products Laboratory, Madison, WI, USA, 2004, p. 73.

Rucka, M. (2011) Damage detection in beams using wavelet transform on higher vibration modes. J. Theor. Appl. Mech. 49:399–417.

Sanabria, S.J., Furrer, R., Neuenschwander, J., Niemz, P., Sennhauser, U. (2011) Air-coupled ultrasound inspection of glued laminated timber. Holzforschung 65:377–387.

Senalik, C.A., Beall, F.C., O'Dell, K., Reis, H. (2008) Detection and assessment of wood decay in glulam beams using a through-transmission ultrasonic approach. In: Proceedings of SPIE, Sensors and Smart Structures Technologies for Civil, Mechanical, and Aerospace Systems 2008, San Diego, CA, USA, Vol. 6932, 69321W-1 to 69321W-12 (12 pages).

Senalik, C.A., Beall, F.C., Reis, H. (2010) Detection and assessment of wood decay in glulam beams using a decay rate approach. Insight- Non-Destructive Testing & Condition Monitoring 52:553–560.

Sitar, M. (2016) Glulam beam repair and strengthening. Civil + Structural Engineer, May feature article http://cenews.com/article/4213/glulam-beam-repair-and-strengthening (accessed on December 22, 2016).

Taha, R.M.M., Noureldin, A., Lucero, J.L., Baca, T.J. (2006) Wavelet transform for structural health monitoring: a compendium of uses and features. Struct. Health Monit. 5:266–295.
Teder, M., Wang, X. (2013) Nondestructive evaluation of a 75-year old glulam arch. In: Proceeding of the 18th International Nondestructive Testing and Evaluation of Wood Symposium, Madison, Wisconsin, USA. pp. 24–27.
Teesdale, L.V. (1935) New building demonstrates modern wood construction. ENR. April 11, 525–527.
Tiitta, M., Biernacki, J.M., and Beall, F.C. (1998) Acousto-ultrasonic assessment of internal decay in glulam beams. Wood Fiber Sci. 30:24–37.
Umesha, P.K., Ravichandran, R., Sivasubramanian, K. (2009) Crack detection and quantification in beams using wavelets. Comput. Aided Civil Infrastruct. Eng. 24:593–607.
Wang, X., Teder, M., Wacker, J. (2013) Condition assessment of the timber structures of a century-old industrial building using a non-destructive inspection procedure. Adv. Mat. Res. 778:840–848.
Xu, F., Liu, Y. (2011) Feature extraction of acoustic emission signal of plywood in loading by wavelet package transform. J. Nanjing Forestry Univ. (Natural Science Edition) 35:101–106.
Xu, F., Liu, Y. (2014) Feature extraction and classification method of acoustic emission signals generated from plywood damage based on EMD-SVD. J. Basic Sci. Eng. 22:1238–1247.